Na_2IrO_3 as a Novel Relativistic Mott Insulator with a 340-meV Gap

R. Comin,[1] G. Levy,[1,2] B. Ludbrook,[1] Z.-H. Zhu,[1] C. N. Veenstra,[1] J. A. Rosen,[1] Yogesh Singh,[3] P. Gegenwart,[4] D. Stricker,[5] J. N. Hancock,[5] D. van der Marel,[5] I. S. Elfimov,[1,2] and A. Damascelli[1,2,*]

[1]*Department of Physics and Astronomy, University of British Columbia, Vancouver, British Columbia V6T 1Z1, Canada*
[2]*Quantum Matter Institute, University of British Columbia, Vancouver, British Columbia V6T 1Z4, Canada*
[3]*Indian Institute of Science Education and Research (IISER) Mohali, Knowledge City, Sector 81, Mohali 140306, India*
[4]*I. Physikalisches Institut, Georg-August-Universität Göttingen, D-37077 Göttingen, Germany*
[5]*Département de Physique de la Matière Condensée, Université de Genève, CH-1211 Genève 4, Switzerland*

(Received 19 April 2012; published 27 December 2012)

We study Na_2IrO_3 by angle-resolved photoemission spectroscopy, optics, and band structure calculations in the local-density approximation (LDA). The weak dispersion of the Ir $5d$-t_{2g} manifold highlights the importance of structural distortions and spin-orbit (SO) coupling in driving the system closer to a Mott transition. We detect an insulating gap $\Delta_{\mathrm{gap}} \simeq 340$ meV which, at variance with a Slater-type description, is already open at 300 K and does not show significant temperature dependence even across $T_N \simeq 15$ K. An LDA analysis with the inclusion of SO and Coulomb repulsion U reveals that, while the prodromes of an underlying insulating state are already found in LDA + SO, the correct gap magnitude can only be reproduced by LDA + SO + U, with $U = 3$ eV. This establishes Na_2IrO_3 as a novel type of Mott-like correlated insulator in which Coulomb and relativistic effects have to be treated on an equal footing.

DOI: 10.1103/PhysRevLett.109.266406 PACS numbers: 71.20.Be, 71.15.Mb, 74.25.Gz, 74.25.Jb

The proposal of an effective $J_{\mathrm{eff}} = 1/2$ Mott-Hubbard state in Sr_2IrO_4 [1] came as a surprise since this case departs from the established phenomenology of Mott-insulating behavior in the canonical early $3d$ transition-metal oxides. There, the localized nature of the $3d$ valence electrons is responsible for the small bandwidth W, large Coulomb repulsion U, and suppression of charge fluctuations [2,3]. In particular, Sr_2IrO_4 appears to violate the $U > W$ Mott criterion, which for the very delocalized $5d$ Ir electrons is not fulfilled. It was proposed that the strong spin-orbit (SO) interaction in $5d$ systems ($\zeta_{\mathrm{SO}} \simeq 485$ meV for Ir [4]) might lead to instability against weak electron-electron correlation effects, and to the subsequent emergence of a many-body insulating ground state [1]. However, the strong-SO limit $J_{\mathrm{eff}} = 1/2$ ground-state scenario has recently been put into question [5], and theoretical [6] and time-resolved optical studies [7] suggest that the insulating state of Sr_2IrO_4 might be closer to a Slater-type than a Mott-type: a bandlike insulating state induced by the onset of antiferromagnetic (AFM) ordering and consequent band folding at $T_N \simeq 240$ K (Slater), as opposed to being driven by correlations with an insulating gap already open at temperatures well above T_N (Mott).

Despite intense experimental and theoretical effort, the nature of the insulating state in the $5d$ iridates remains highly controversial. This is reminiscent of the situation in $3d$ oxides, for which the Mott versus band-insulator debate has lasted over four decades [2,8–10]. For instance, in the case of the prototypical AFM insulator NiO, this debate was conclusively resolved only after the correlated nature of the insulating state was established based on (i) the magnitude of the gap as measured by direct and inverse photoelectron spectroscopy (PES, IPES) [11], much larger than expected from density functional theory (DFT) [8]; (ii) its persistence well above the Néel temperature T_N [12]; and (iii) the detailed comparison between dynamical mean-field theory results [13] and momentum-resolved electronic structure as measured by angle-resolved photoelectron spectroscopy (ARPES) [12,14].

To address the nature of the insulating state in iridates, including the role of many-body electron correlations for their extended $5d$ orbitals and the delicate interplay between W, U and SO energy scales, a particularly interesting system is the newly discovered AFM insulator Na_2IrO_3 [15]. Starting from a $J_{\mathrm{eff}} = 1/2$ model in analogy with Sr_2IrO_4, this system was predicted to exhibit quantum spin Hall behavior, and was considered a potential candidate for a topologically insulating state [16]. Further theoretical [17,18] and experimental [19] work emphasized the relevance of structural distortions, which lower the local symmetry at the Ir site from octahedral (O_h) to trigonal (D_{3h}). Together with the structure comprised of edge-sharing IrO_6 octahedra, this leads to an effective bandwidth for the Ir $5d$-t_{2g} manifold of $\sim$1 eV. This potentially puts Na_2IrO_3 closer than other iridates to the $U \sim W$ Mott criterion borderline—and thus to a Mott insulating phase [17]. Most importantly, its lower $T_N \simeq 15$ K provides the opportunity of studying the electronic structure well above the long-range AFM ordering temperature and—with the aid of novel DFT calculations—establishing the nature of its insulating behavior.

In this Letter, we present a study of the low-energy electronic structure of Na_2IrO_3 by ARPES, angle-integrated PES with *in situ* potassium doping, optics, and DFT

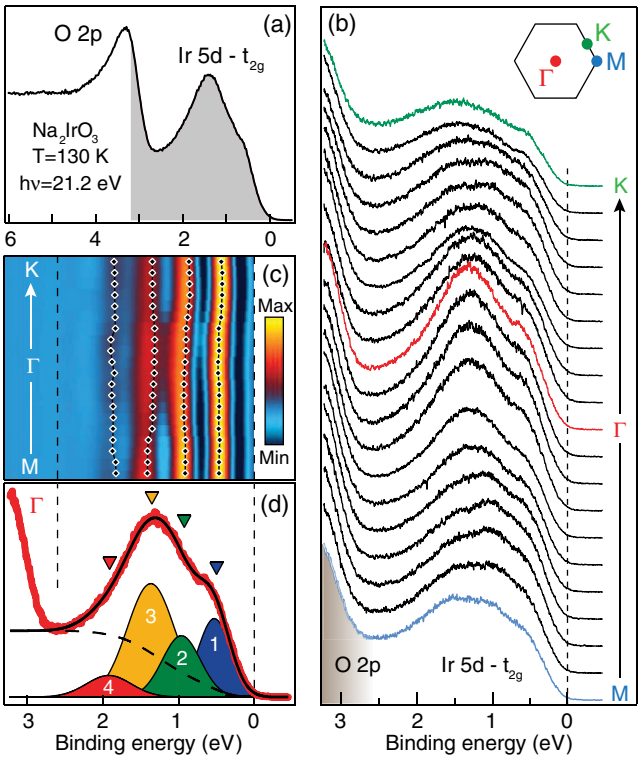

FIG. 1 (color online). (a) Angle-integrated O and Ir valence-band photoemission spectrum of Na_2IrO_3; the grey portion is shown in detail in (b)–(d). (b) ARPES EDCs for the Ir $5d$-t_{2g} bands from along M-Γ-K. (c) Negative second derivative of the ARPES map highlighting the experimental dispersion; superimposed (black diamonds) are the fit analysis results from (d). (d) Model fit of the Γ-point EDC with 4 Gaussian peaks for the Ir VBs and a Shirley background [23]: 4 peaks are necessary to fit the data set over the full momentum range [matching the number of DOS features from DFT in Figs. 4(e) and 4(f)], with Gaussian line shapes yielding better agreement than Lorentzians. The average over $M-\Gamma-K$ gives (E_{VB}, Γ_{VB}, ΔE_{VB}) in eV, for peaks 1 to 4: (0.50, 0.30, 0.06); (0.94, 0.39, 0.08); (1.39, 0.44, 0.09); (1.89, 0.43, 0.07).

calculations in the local-density approximation (LDA). The narrow bandwidth of the Ir $5d$ manifold observed in ARPES highlights the importance of SO and structural distortions in driving the system toward a Mott transition. In addition, at variance with a Slater-type description, the gap is already open at 300 K and does not show significant temperature dependence even across $T_N \simeq 15$ K. From the potassium-induced chemical potential shift and complementary optical conductivity measurements, we estimate the insulating gap to be $\Delta_{gap} \simeq 340$ meV. While LDA + SO already returns a depletion of density of states (DOS) at E_F, this only corresponds to a "zero gap." The observed 340 meV gap value can be reproduced only in LDA + SO + U calculations, i.e., with *the inclusion of both SO and U* (with $U \simeq 3$ eV), establishing Na_2IrO_3 as a novel *relativistic Mott insulator.*

The 130 K angle-integrated PES spectrum [20] in Fig. 1(a) shows two broad spectral features belonging to the Ir $5d$-t_{2g} bands (0–3 eV binding energy), and to the O $2p$ manifold (beyond 3 eV). The insulating character is evidenced by the lack of spectral weight at the chemical potential, which appears to be pinned to the top of the valence band (no temperature dependence is observed in the 130–250 K range [20,21]). Energy distribution curves (EDCs) measured by ARPES [20] along M-Γ-K for the Ir $5d$-t_{2g} bands are shown in Fig. 1(b). The detected features are only weakly dispersing in energy, with the most obvious momentum dependence being limited to their relative intensity. The electronic dispersion can be estimated from the negative second derivative map in Fig. 1(c), calculated as $-\partial^2 I(\mathbf{k}, E)/\partial E^2$, and more quantitatively from the fit of EDCs as in Fig. 1(d) (see caption for details). The direct comparison of fit (black diamonds) and second derivative results in Fig. 1(c) yields a good overall agreement in the dispersion of the 4 features (small deviations stem from the peaks' relative intensity variation, which is differently captured by the two methods). We find that the Ir $5d$-t_{2g} valence band (VB) dispersions do not exceed $\Delta E_{VB} \sim 100$ meV in bandwidth—at variance with the generally expected larger hopping amplitude for $5d$-t_{2g} states. Another remarkable aspect of the Ir t_{2g} bands is their linewidth, with values $\Gamma_{VB} = \sqrt{2}\sigma_{VB} \sim$ 300–450 meV. A possible origin might be many-body electron correlation effects as discussed for NiO [13], and strong electron-phonon coupling leading to polaronic behavior in the spectral function [22].

The results in Fig. 1 already provide one very important clue: the gap is open well above $T_N \simeq 15$ K, which directly excludes a Slater-type, magnetic-order-driven nature for the insulating state. As for the size of the gap, this cannot be readily identified by ARPES since photoemission can locate the valence band, as the first electron-removal state, but not the conduction band which belongs to the electron-addition part of the spectral function [23]. Alternatively, one can measure the gap in an optical experiment; however, one needs to discriminate between in-gap states of bosonic character (e.g., phonons, magnons, excitons) and those particle-hole excitations which instead determine the real charge gap. This complication can often hinder the precise identification of the gap edge [24]. Such complexity underlies the past controversy on NiO: while the 0.3 eV gap obtained by DFT [8] was deemed to be consistent with optical experiments [25], the combination of direct and inverse PES revealed the actual gap value to be 4.3 eV [11]. This is well beyond the DFT estimate and establishes NiO as a correlated insulator. Here, for the most conclusive determination of the insulating gap magnitude, we use angle-integrated PES with *in situ* doping by potassium deposition, as well as optics. A quantitative agreement between the two probes would provide validation against possible artifacts [26].

To estimate the energy of the first electron-addition states and the DOS gap between valence and conduction bands, we start by doping carriers (i.e., electrons) across the gap by *in situ* potassium deposition on the cleaved surfaces, and then follow the shift in chemical potential

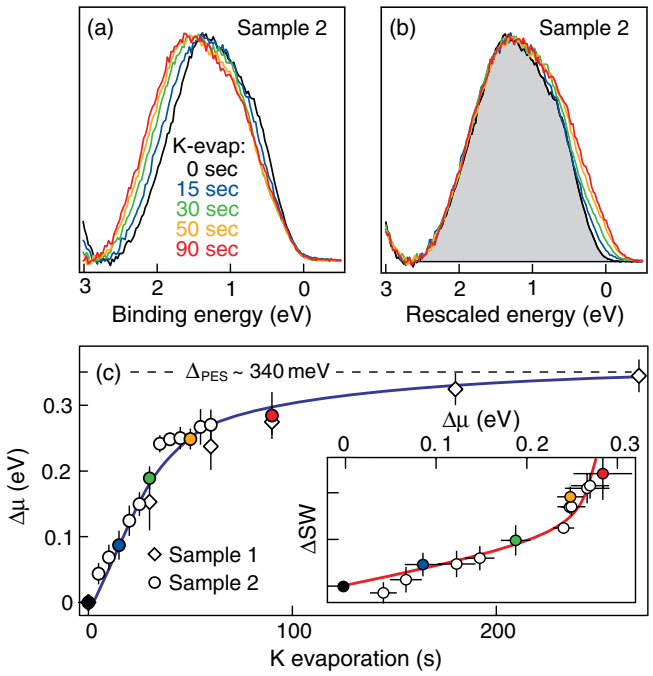

FIG. 2 (color online). (a) Background-subtracted angle-integrated EDCs for selected values of K-exposure [see colored markers in (c)]; the chemical potential shift $\Delta\mu$ is revealed by the motion of the high binding-energy trailing edge. (b) Same as in (a), but shifted by the corresponding $\Delta\mu$. (c) $\Delta\mu$ versus the K-deposition time for two different samples; in the inset, K-induced low-energy spectral weight ΔSW as a function of $\Delta\mu$, for Sample 2 only. In panel (c) data and error bars are estimated from the comprehensive analysis of both O and Ir trailing edges and peak positions [21]; also note that blue and red curves in (c) and its inset are both a guide-to-the-eye.

by angle-integrated PES. The results are summarized in Fig. 2 for K-evaporation performed at 130 K on two different freshly cleaved surfaces [27]. The most evident effect is the shift toward higher binding energy of both Ir and O valence bands, as shown in Fig. 2(a) for the Ir $5d$-t_{2g} manifold [21]. This arises from the (equal and opposite) shift of the chemical potential $\Delta\mu$ when electrons donated by potassium are doped into the system; after an initial rapid increase, $\Delta\mu$ saturates at ~340 meV [Fig. 2(c)]. When the K-deposited spectra are shifted in energy by the corresponding $\Delta\mu$ so that their high binding-energy trailing edges match the one of the fresh surface [Fig. 2(b)], one can observe the emergence of additional spectral weight (SW) in the region close to and above E_F. This low-energy K-induced spectral weight, ΔSW, can be computed as

$$\Delta\mathrm{SW} = \int dk \int_{-1eV}^{E_F^+} dE[I(k, E, x_{K^+}) - I(k, E, 0)], \quad (1)$$

where $I(k, \omega)$ is the PES intensity, x_{K^+} represents the K-induced surface doping, and E_F^+ is the Fermi energy of the K-doped surface, which moves progressively beyond E_F value for the undoped surface. The evolution of ΔSW plotted versus $\Delta\mu$ in the inset of Fig. 2(c) evidences an approximately linear SW increase up to $\Delta\mu \simeq$ 200–250 meV, followed by a steeper rise once the saturation value $\Delta\mu \simeq 340$ meV is being approached. This behavior can be understood as due to the initial filling in of in-gap defect states—either preexisting or induced by K-deposition—which makes the jump of the chemical potential not as sudden as for a clean insulating DOS. Only when electronic states belonging to the Ir $5d$-t_{2g} conduction band are reached one observes the saturation of $\Delta\mu$ and the more pronounced increase in ΔSW. This combined evolution of chemical potential shift and spectral weight increase points to a DOS insulating gap $\Delta_{PES} \simeq 340$ meV.

Turning now to the optical conductivity data [28], in Fig. 3 we observe an insulating behavior with an absorption edge starting at 300–400 meV at 300 K, with negligible temperature dependence down to 8 K and thus also across $T_N \simeq 15$ K (see inset). We can fit the results using a joint DOS with Gaussian peaks for the conduction band (CB) and each of the 4 VBs (see caption of Fig. 1):

$$J(E) \propto \sum_{i=1}^{4} \int dE' A_i G_{\mathrm{CB}}(E' + E) G_{\mathrm{VB}i}(E'). \quad (2)$$

Here the prefactors A_i represent the optical transition strengths, with the band index i running over the 4 VB features extracted from the ARPES data in Fig. 1, and are left free. $J(E)$ provides an excellent fit to the optical data in Fig. 3, and a least-squares analysis returns $E_{\mathrm{CB}} \simeq 680$ meV for the location of the conduction band above E_F, with a width $\Gamma_{\mathrm{CB}} = \sqrt{2}\sigma_{\mathrm{CB}} \simeq 160$ meV (a value in agreement with DFT, as shown later). The consistency of the

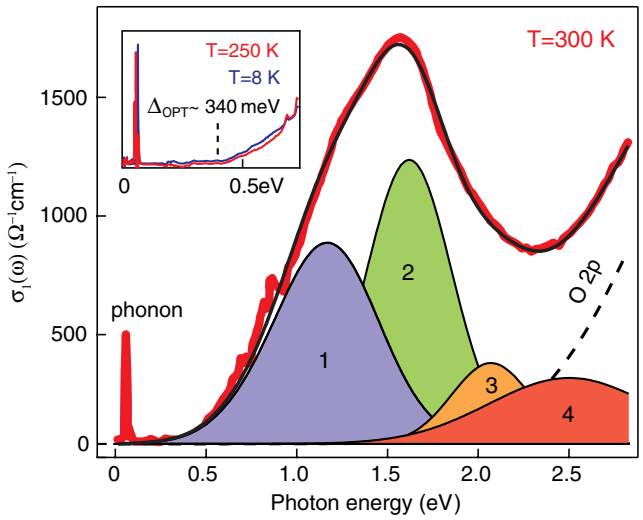

FIG. 3 (color online). Optical conductivity data (red line), together with the simulated Ir $5d$-t_{2g} joint particle-hole DOS (black line), and its individual components from the simultaneous fit of ARPES and optical data [colors and labels are consistent with the valence band features in Fig. 1(c), which represent the initial states of the lowest-energy optical transitions]. Inset: Temperature dependence of the gap edge.

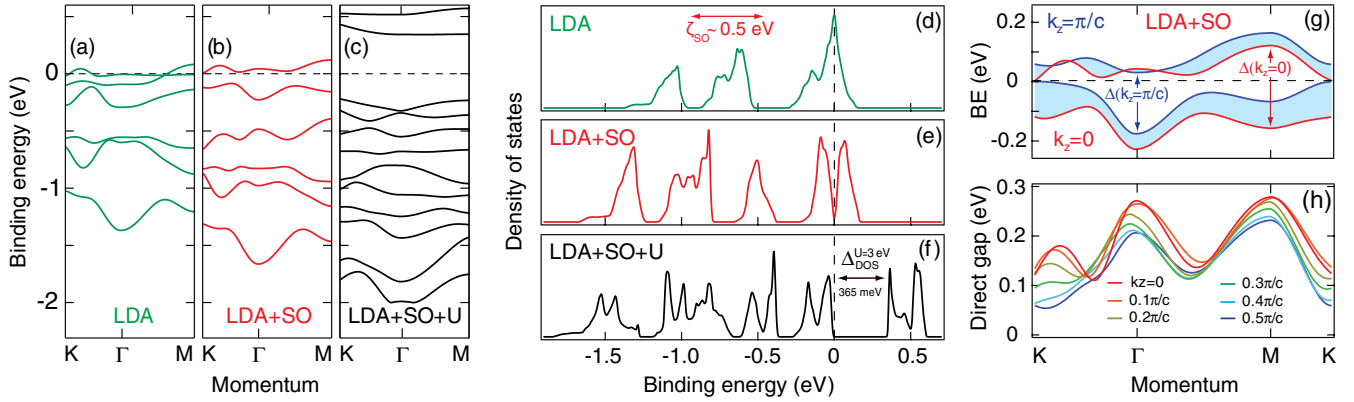

FIG. 4 (color online). (a)–(c) Ir $5d$ t_{2g} band structure ($k_z = 0$), and (d)–(f) corresponding DOS, obtained with LDA, LDA + SO, and LDA + SO + U ($U = 3$ eV, $J_H = 0.6$ eV [38]). (g) k_z dispersion for the last occupied and first unoccupied Ir $5d$-t_{2g} bands from LDA + SO, as indicated by the filled region between the $k_z = 0$ and π/c extreme lines. While the filled areas overlap, resulting in a vanishing indirect gap (i.e., $\Delta k \neq 0$), the direct gap (i.e., $\Delta k = 0$) between valence and conduction bands is finite for all k_z and $k_\parallel$. (h) LDA + SO direct gap distribution along M-Γ-K, for different k_z in the 3-dimensional Brillouin zone.

combined PES-optical conductivity analysis is confirmed by the optical gap obtained from the onset of the simulated conduction band, $\Delta_{\rm OPT} = E_{\rm CB}^{\rm onset}$. Following Ref. [22], the latter is estimated as $E_{\rm CB}^{\rm onset} = E_{\rm CB} - 3\sigma_{\rm CB}$, leading to $\Delta_{\rm OPT} \simeq 340$ meV. This matches $\Delta_{\rm PES}$ from the K-induced $\Delta\mu$ saturation in PES, providing a definitive estimate for the insulating gap, $\Delta_{\rm gap} \simeq 340$ meV.

With a gap much smaller than in typical Mott insulators, discriminating between correlated and bandlike insulating behavior in Na_2IrO_3 requires a detailed comparative DFT analysis [29]. Unlike the case of Sr_2IrO_4, the t_{2g} degeneracy and bandwidth in Na_2IrO_3 are affected by structural distortions and the presence of Na in the Ir plane. This is revealed by calculations we have performed for a distortion- and Na-free hypothetical IrO_2 parent compound: while in IrO_2 the individual t_{2g} dispersions are as wide as ~1.6 eV, the Na-induced band folding in Na_2IrO_3 opens large band gaps, leading to much narrower t_{2g} subbands (~ 100 meV). Even though this accounts well for the narrow bandwidth observed in ARPES, the material is still metallic in LDA with a high DOS at the Fermi level [Figs. 4(a) and 4(d)], at variance with the experimental findings. between observed and SO is switched on in LDA + SO a clear gap opens up at E_F in the $k_z = 0$ band dispersion [Fig. 4(b)], although not in the DOS where only a *zero gap* can be observed [Fig. 4(e)]. A closer inspection of the LDA+SO dispersion for first occupied and unoccupied bands—versus both $k_\parallel$ and k_z in Fig. 4(g)—reveals that the lack of a DOS gap stems from the overlap of VB and CB at Γ and K points for different k_z values. In other words, while the *direct* gap ($\Delta k = 0$) is nonzero and ranges from a minimum of 54 meV to a maximum of 220 meV over the full Brillouin zone [Fig. 4(h)], the *indirect* DOS gap ($\Delta k \neq 0$) is vanishing. This is still in contrast with the experimentally determined band-gap magnitude $\Delta_{\rm gap} \simeq 340$ meV [37].

The disconnection between insulating behavior and the onset of AFM ordering, together with the quantitative disagreement between observed and calculated gap even in LDA + SO, reveal that Na_2IrO_3 cannot be regarded as either a Slater or a band insulator. Also, given the narrow t_{2g} bandwidths (~ 100 meV), one might expect the system to be even more unstable against local correlations than anticipated. Indeed, a good overall agreement with the data is found in LDA + SO + U, for $U = 3$ eV and $J_H = 0.6$ eV [38]: this returns a gap value $\Delta_{\rm DOS}^{U=3{\rm eV}} \simeq 365$ meV [Fig. 4(f)] close to the experimental $\Delta_{\rm gap}$, and a 2 eV energy range for the Ir $5d$ t_{2g} manifold [Fig. 4(c)] matching the spectral weight distribution in Fig. 1 (note that a doubling of bands is seen in LDA + SO + U due to the imposed AFM ordering, but is of no relevance here [29]). At a first glance, $U = 3$ eV might seem a large value for $5d$ orbitals; however, in the solid, the effective reduction of the atomic value of U strongly depends on the polarizability of the surrounding medium, which is the result of many factors, *in primis* the anion-cation bond length [39]. In this perspective, the value we found is not unreasonable, and is also consistent with the existence of local moments above T_N revealed by the Curie-Weiss magnetic susceptibility behavior with $\theta \simeq -120$ K [15].

Our findings point to a Mott-like insulating state driven by the delicate interplay between W, U, and SO energy scales, in which coparticipating structural distortions also play a crucial role. This establishes Na_2IrO_3, and possibly other members of the iridate family, as a novel type of correlated insulator in which many-body (Coulomb interaction) and relativistic (spin-orbit coupling) effects cannot be decoupled, but must be treated on an equal footing.

We acknowledge S. Bhattacharjee and G. A. Sawatzky for discussions, and D. Wong and P. Dosanjh, for technical assistance. This work was supported by the Max Planck-UBC Centre for Quantum Materials, the Killam, Sloan, von Humboldt, and NSERC's Steacie Fellowship Programs (A. D.), the Canada Research Chairs Program, NSERC, CFI, and CIFAR Quantum Materials.

*damascelli@physics.ubc.ca

[1] B. J. Kim, H. Jin, S. J. Moon, J.-Y. Kim, B.-G. Park, C. S. Leem, J. Yu, T. W. Noh, C. Kim, S.-J. Oh, J.-H. Park, V. Durairaj, G. Cao, and E. Rotenberg, Phys. Rev. Lett. **101**, 076402 (2008).

[2] N. F. Mott, Proc. Phys. Soc. London Sect. A **62**, 416 (1949).

[3] J. Zaanen, G. A. Sawatzky, and J. W. Allen, Phys. Rev. Lett. **55**, 418 (1985).

[4] M. Montalti, A. Credi, L. Prodi, and M. T. Gandolfi, *Handbook of Photochemistry* (CRC Press Taylor and Francis Group, Boca Raton, FL, 2006), 3rd ed.

[5] D. Haskel, G. Fabbris, M. Zhernenkov, P. P. Kong, C. Q. Jin, G. Cao, and M. van Veenendaal, Phys. Rev. Lett. **109**, 027204 (2012).

[6] R. Arita, J. Kuneš, A. V. Kozhevnikov, A. G. Eguiluz, and M. Imada, Phys. Rev. Lett. **108**, 086403 (2012).

[7] D. Hsieh, F. Mahmood, D. H. Torchinsky, G. Cao, and N. Gedik, Phys. Rev. B **86**, 035128 (2012).

[8] K. Terakura, A. R. Williams, T. Oguchi, and J. Kübler, Phys. Rev. Lett. **52**, 1830 (1984).

[9] A. Fujimori, F. Minami, and S. Sugano, Phys. Rev. B **29**, 5225 (1984).

[10] A. Fujimori and F. Minami, Phys. Rev. B **30**, 957 (1984).

[11] G. A. Sawatzky and J. W. Allen, Phys. Rev. Lett. **53**, 2339 (1984).

[12] O. Tjernberg, S. Söderholm, G. Chiaia, R. Girard, U. O. Karlsson, H. Nylén, and I. Lindau, Phys. Rev. B **54**, 10245 (1996).

[13] J. Kuneš, V. I. Anisimov, S. L. Skornyakov, A. V. Lukoyanov, and D. Vollhardt, Phys. Rev. Lett. **99**, 156404 (2007).

[14] Z.-X. Shen, C. K. Shih, O. Jepsen, W. E. Spicer, I. Lindau, and J. W. Allen, Phys. Rev. Lett. **64**, 2442 (1990).

[15] Y. Singh and P. Gegenwart, Phys. Rev. B **82**, 064412 (2010).

[16] A. Shitade, H. Katsura, J. Kuneš, X.-L. Qi, S.-C. Zhang, and N. Nagaosa, Phys. Rev. Lett. **102**, 256403 (2009).

[17] H. Jin, H. Kim, H. Jeong, C. H. Kim, and J. Yu, arXiv:0907.0743v1.

[18] S. Bhattacharjee, S.-S. Lee, and Y. B. Kim, New J. Phys. **14**, 073015 (2012).

[19] F. Ye, S. Chi, H. Cao, B. C. Chakoumakos, J. A. Fernandez-Baca, R. Custelcean, T. F. Qi, O. B. Korneta, and G. Cao, Phys. Rev. B **85**, 180403 (2012).

[20] ARPES measurements were performed at UBC with 21.2 eV linearly polarized photons (He-Iα line from a SPECS UVS300 monochromatized lamp) and a SPECS Phoibos 150 hemispherical analyzer. Energy and angular resolutions were set to 30 meV and 0.2°. Na_2IrO_3 single crystals were grown by a self-flux method [15] and preoriented by Laue diffraction, and then cleaved *in situ* at a base pressure of 5×10^{-11} mbar, exposing the (001) surface (parallel to the Ir layers). During all measurements, the temperature was kept at 130 K to guarantee stable conditions for as-cleaved and K-deposited surfaces (lower temperatures were prevented by the onset of charging [21]).

[21] See Supplemental Material at http://link.aps.org/supplemental/10.1103/PhysRevLett.109.266406 for additional details on K-evaporation procedure, temperature dependence and treatment of charging effects.

[22] K. M. Shen, F. Ronning, D. H. Lu, W. S. Lee, N. J. C. Ingle, W. Meevasana, F. Baumberger, A. Damascelli, N. P. Armitage, L. L. Miller, Y. Kohsaka, M. Azuma, M. Takano, H. Takagi, and Z.-X. Shen, Phys. Rev. Lett. **93**, 267002 (2004).

[23] A. Damascelli, Phys. Scr. **T109**, 61 (2004).

[24] D. N. Basov, R. D. Averitt, D. van der Marel, M. Dressel, and K. Haule, Rev. Mod. Phys. **83**, 471 (2011).

[25] R. Newman and R. M. Chrenko, Phys. Rev. **114**, 1507 (1959).

[26] Stemming from excitonic contamination in optics and/or surface sensitivity in PES, including effects specific to the substrate-adsorbate system in PES with *in situ* doping.

[27] Potassium was evaporated at a constant rate and in steps of equal exposure, with the following evaporation current per time: $I_{\mathrm{evap}} = 4.2\,\mathrm{A}/5\,\mathrm{s}$ for sample 1; $I_{\mathrm{evap}} = 4.5\,\mathrm{A}/30\,\mathrm{s}$ for sample 2. Note that no K-desorption between consecutive steps was observed, a sign of the stability of the evaporated surfaces at these temperatures; and also no detectable change in angle-to-momentum relations, and correspondingly of work function.

[28] The complex optical conductivity was obtained in the 8–300 K temperature range using combined reflectivity and ellipsometry measurements on the (001) surface of a freshly cleaved crystalline platelet.

[29] We have performed band-structure calculations using the linearized augmented plane wave method in WIEN2K [30], and the most recently refined monoclinic $C2/m$ crystal structure with 2 formula units per unit cell [31]. Exchange and correlation effects were treated within the generalized gradient approximation [32]; SO was included as a second variational step using eigenfunctions from a scalar relativistic calculation [33]. The LDA + U method was applied to the Ir 5d states by varying U from 1 to 5 eV [34] with $J_H = 0.6$ eV [35], and adopting the zigzag antiferromagnetic spin arrangement with moments along the a axis (zigzag a) [36].

[30] P. Blaha, K. Schwarz, G. Madsen, D. Kvasnicka, and J. Luitz, in *An Augmented Plane Wave Plus Local Orbitals Program for Calculating Crystal Properties*, edited by K. Schwarz (Technical University of Wien, Vienna, 2001).

[31] S. K. Choi, R. Coldea, A. N. Kolmogorov, T. Lancaster, I. I. Mazin, S. J. Blundell, P. G. Radaelli, Y. Singh, P. Gegenwart, K. R. Choi, S.-W. Cheong, P. J. Baker, C. Stock, and J. Taylor, Phys. Rev. Lett. **108**, 127204 (2012).

[32] J. P. Perdew, K. Burke, and M. Ernzerhof, Phys. Rev. Lett. **77**, 3865 (1996).

[33] A. H. MacDonald, W. E. Picket, and D. D. Koelling, J. Phys. C **13**, 2675 (1980).

[34] V. I. Anisimov, I. V. Solovyev, M. A. Korotin, M. T. Czyżyk, and G. A. Sawatzky, Phys. Rev. B **48**, 16929 (1993).

[35] D. van der Marel and G. A. Sawatzky, Phys. Rev. B **37**, 10674 (1988).

[36] X. Liu, T. Berlijn, W.-G. Yin, W. Ku, A. Tsvelik, Y.-J. Kim, H. Gretarsson, Y. Singh, P. Gegenwart, and J. P. Hill, Phys. Rev. B **83**, 220403 (2011).

[37] PES with K doping provides a measure of the indirect DOS gap, while optics probes the direct optical gap averaged over the whole three-dimensional Brillouin zone.

[38] This choice corresponds to $U_{\mathrm{eff}} = U - J_H = 2.4$ eV, which is consistent with the value $U_{\mathrm{eff}} = 2$ eV used in Ref. [17].

[39] M. B. J. Meinders, J. van den Brink, J. Lorenzana, and G. A. Sawatzky, Phys. Rev. B **52**, 2484 (1995).

Auxiliary Material for EPAPS:

Na_2IrO_3 as a Novel Relativistic Mott Insulator with a 340 meV Gap

R. Comin, G. Levy, B. Ludbrook, Z.-H. Zhu, C.N. Veenstra, J.A. Rosen, Yogesh Singh, P. Gegenwart, D. Stricker, J.N. Hancock, D. van der Marel, I.S. Elfimov, and A. Damascelli

SI I. Temperature dependence and charging effects in PES

Charging effects are a well-known hindrance in photoelectron spectroscopy, as they can produce extrinsic artifacts in the spectra. They arise whenever the (positive) charge build-up at the surface, due to the photoelectric effect, is not compensated by neutralizing carriers supplied through the ohmic contact between sample and spectrometer. Charging is triggered not only by temperature (making insulating samples exponentially more resistive) but also by photon flux (more electrons are being pulled out as light intensity is increased).

Concerning our ARPES and PES measurements, we have employed two approaches to ensure that we are confidently safe from charging effects. (i) We studied the temperature dependence from 300 K down to 70 K on a series of different surfaces in order to establish a safe temperature range for subsequent measurements (see main panel in Fig. S1); this way we selected 130 K as the optimal lowest temperature for our study. (ii) For all measurements performed at 130 K, before starting with extended acquisitions we also measured angle-integrated photoemission spectra as a function of photon flux (see Fig. S2), as an additional check against charging (prior to and during evaporation the sample temperature was kept extremely stable, hence we could not check for charging via cooling).

In particular, from Fig. S1 it can be seen that: (i) down to 125 K no charging is taking place (the curves at 150 and 125 K overlap almost perfectly); (ii) at 95 K (blue curve) the spectrum gets broader and shifts downwards in binding energy. These are two distinctive

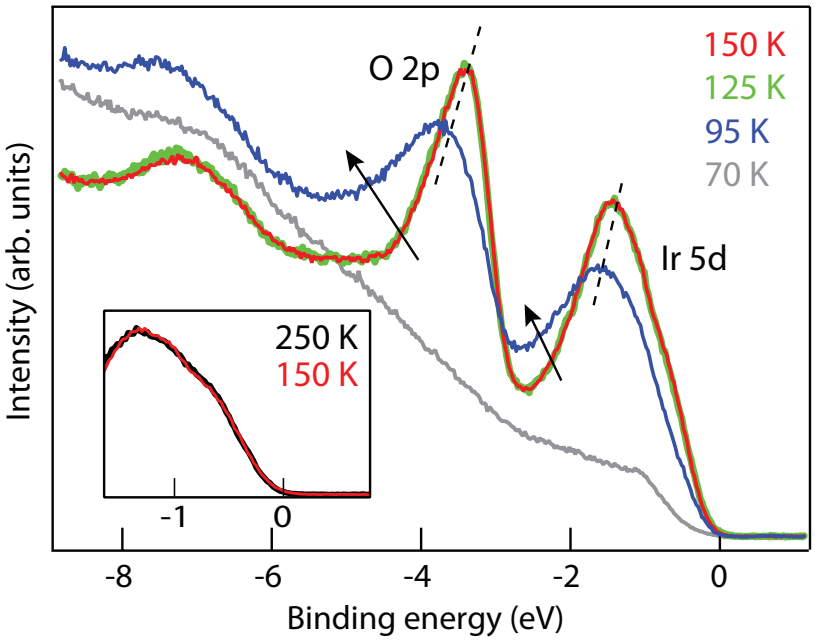

Fig. S1: Angle-integrated photoemission (PES) spectra from around Γ-point and up to 9 eV in binding energy plotted for various temperatures: from 150 to 70 K (main panel) to show the onset of charging below 120 K, and for 150 and 250 K (inset) to highlight the lack of temperature dependence in the low-energy leading ege.

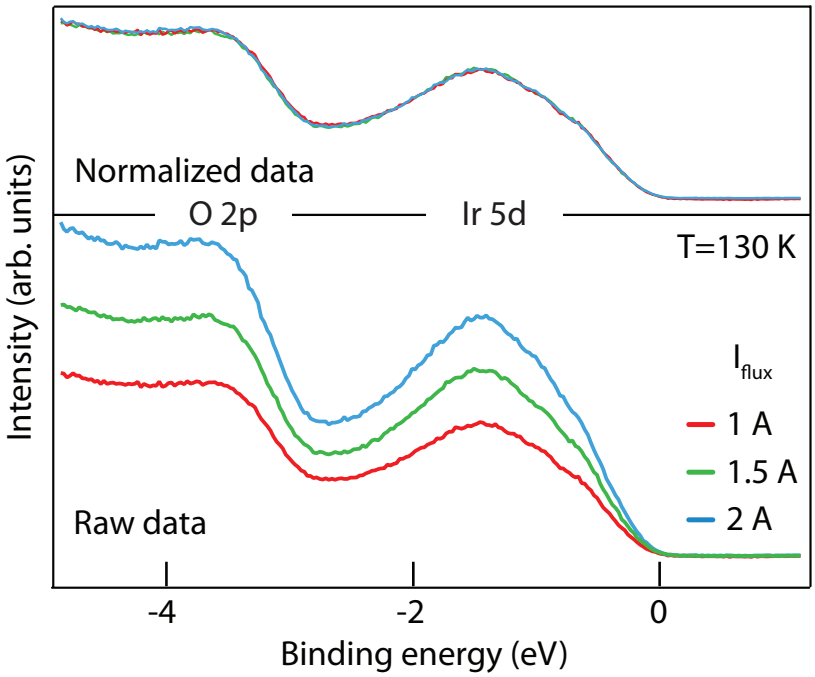

Fig. S2: PES spectra at T =130 K, as a function of photon flux (parametrized using the He lamp anode current: raw spectra (bottom), and normalized to the total area (top).

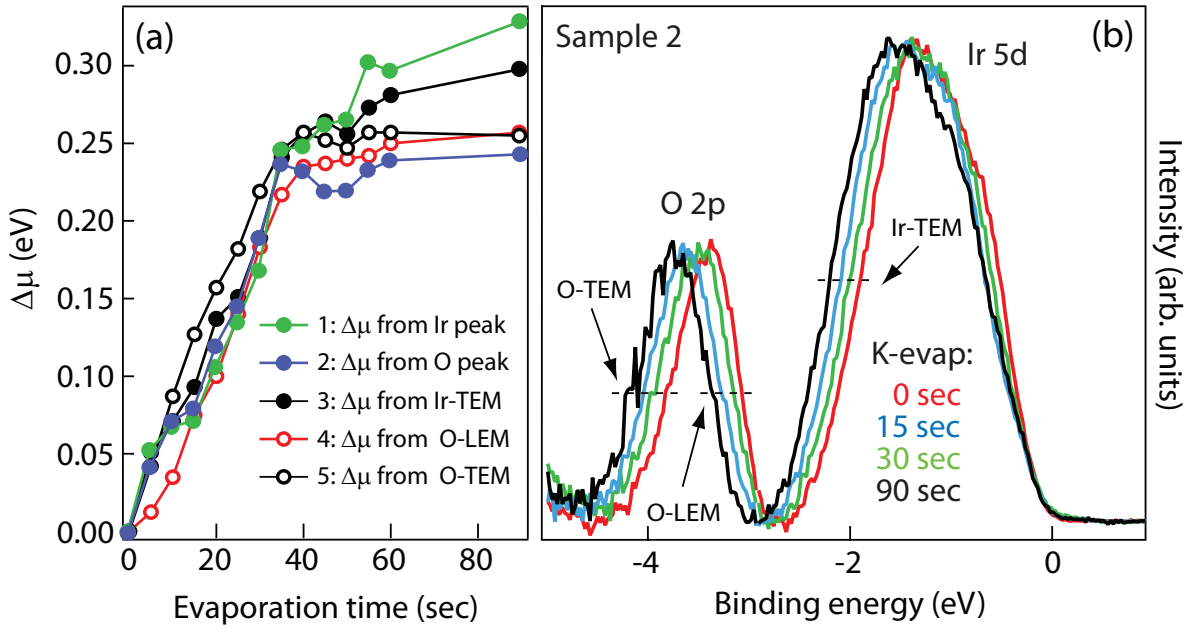

Fig. S3: Main panel: background-subtracted angle-integrated PES spectra showing both Ir-5d and O-2p manifolds, for selected values of potassium deposition, taken at T = 130 K on Sample 2 (same sample as in Fig. 2 of the main body of the paper). Top-left panel: plot of $\Delta\mu$ as extrapolated from the 5 different procedures discussed in the text.

signatures (broadening + shift) of spectral weight being inhomogeneously moved to higher binding energies due to charging. In addition, we also show a profile taken at 70 K (grey curve), where charging effects are so severe that all the valence band features are completely washed away. At 130 K, we never observed any indication of charging; this is demonstrated by the lack of any variation in angle-integrated PES spectra taken upon reducing the photon flux on the sample, once the spectra have been normalized to compensate for the corresponding drop in intensity (Fig. S2). This allowed us to verify that charging effects could be ruled out for all measurements performed at 130 K – on both as-cleaved as well as K-deposited surfaces.

One last important insight obtained from these temperature dependent measurements is that the PES spectra exhibit no intrinsic temperature dependence in the range 250-130 K. An enlarged view of the leading edge of the angle-integrated PES spectra between 250 and 150K is shown in the inset of Fig. S1. This highlights the lack of any temperature dependence in PES, consistent with what is observed also in optics all the way down to 8 K (see Fig. 3 in the main text), in stark contrast with what is expected for a Slater-type insulating state.

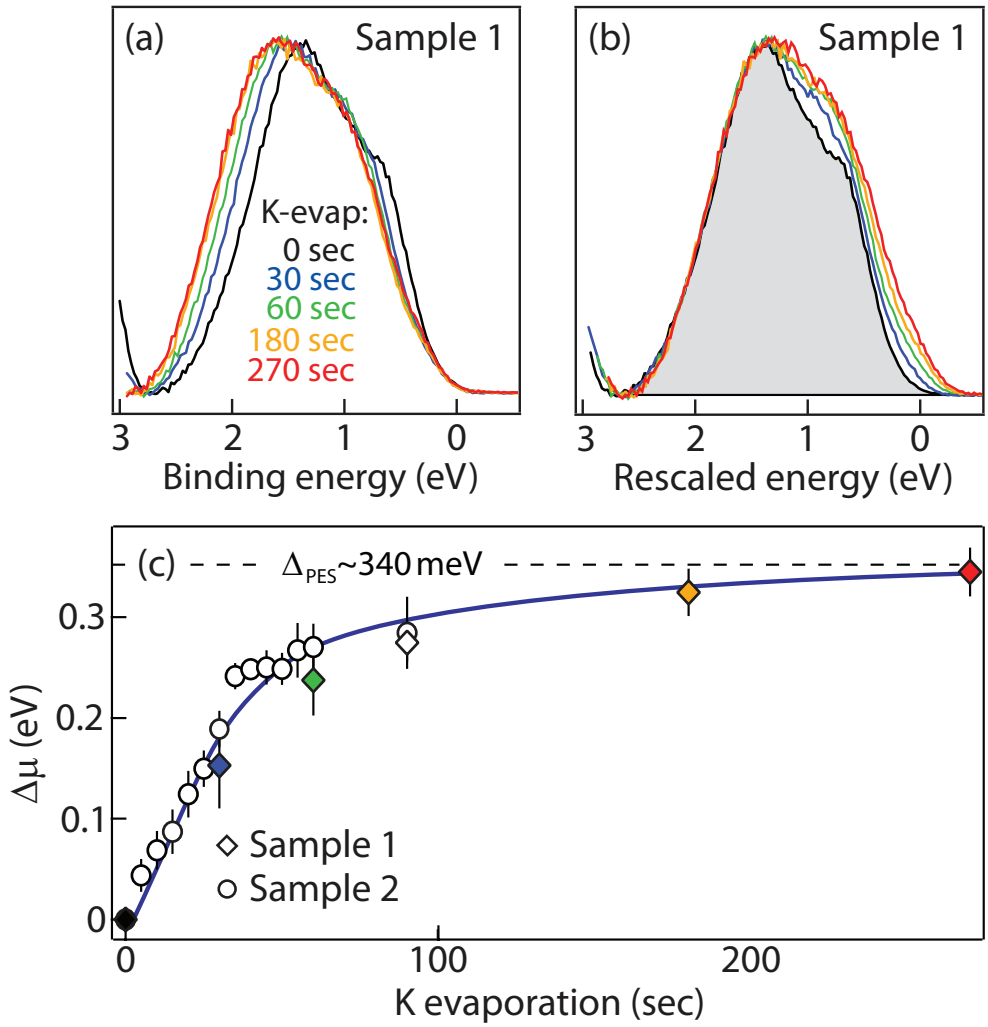

Fig. S4: (a) Background-subtracted angle-integrated PES spectra from Sample 1, for selected values of K-deposition [see colored markers in (c)]; the chemical potential shift $\Delta\mu$ is evidenced by the shift of the high binding-energy trailing edges. (b) Same as in (a), but shifted by the corresponding $\Delta\mu$. (c) $\Delta\mu$ vs. K-deposition time for two different samples.

SI II. Extraction of $\Delta\mu$ from PES with K-doping

Potassium was evaporated from a commercial SAES alkali-metal dispenser, at a constant rate and in steps of equal exposure, with the following evaporation current/time: $I_{evap} = 4.2\,\mathrm{A}/5\,\mathrm{sec}$ for sample 1; $I_{evap} = 4.5\,\mathrm{A}/30\,\mathrm{sec}$ for sample 2. Note that no K desorption between consecutive steps was observed, a sign of the stability of the evaporated surfaces at these temperatures; and also no detectable change in angle-to-momentum relations, and correspondingly of work-function.

The data points corresponding to the chemical potential shift $\Delta\mu$ (as in Fig. 2, main text) have been extracted in a variety of ways. Fig. S3 showcases the different methods we employed, which are based on the analysis of the angle-integrated ARPES curves as a function of potassium evaporation (see panel (b) in Fig. S3), for the case of Sample 2 (the same analysis was applied to Sample 1). Based on the idea that a chemical potential shift drives a *rigid* downwards energy shift of all bands, quantitative estimates for $\Delta\mu$ have been extracted from the shift of the intensity maximum (peak) of the Ir-5d (1) and O-2p (2) manifold, the trailing-edge-midpoint (TEM) of the Ir-5d (3) and O-2p (4) manifold, and the leading-edge-midpoint (LEM) of the O-2p manifold (5). Note that the Ir-5d LEM cannot be used for this analysis as it lies in an energy region where new states are populated with increasing potassium coverage. Panel (a) in Fig. S3 plots the values corresponding to the above-listed quantities, as a function of K-evaporation time. It is apparent how the data have a bit of a scatter, which we used to statistically define $\Delta\mu$ and its error $\delta_{\Delta\mu}$ in Fig. 2(c) in the main text, as the average and standard deviation over the different methods employed.

As a last element, we show the full dataset for K-evaporation on Sample 1. These results are presented in Fig. S4, which is the exact analogue of Fig. 2 in the main article and allows following the saturation of $\Delta\mu$ upon approaching the highest K-deposition.